ELEMENTA
Science of the Anthropocene

Rogener, MK, et al. 2018 Long-term impact of the Deepwater Horizon oil well blowout on methane oxidation dynamics in the northern Gulf of Mexico. *Elem Sci Anth,* 6: 73. DOI: https://doi.org/10.1525/elementa.332

RESEARCH ARTICLE

Long-term impact of the Deepwater Horizon oil well blowout on methane oxidation dynamics in the northern Gulf of Mexico

Mary Katherine Rogener*, Annalisa Bracco†, Kimberley S. Hunter*, Matthew A. Saxton* and Samantha B. Joye*

The Deepwater Horizon oil well blowout discharged an unprecedented amount of methane into the water column of the northern Gulf of Mexico between April and July 2010. The methanotrophic community bloomed in response to the sustained methane release, resulting in the highest methane oxidation rates measured in the water column of an open ocean environment to date. To assess the long-term impact and recovery of the northern Gulf of Mexico methanotrophic community, we tracked methane dynamics for five years post-blowout. We determined methane concentration and methane oxidation rates at 31 different sites, resulting in ~900 discrete water column samples across the northern Gulf ecosystem, the largest compilation of methane oxidation rate measurements in an offshore ocean environment. Though methane concentrations approached pre-blowout concentrations within one year, methane oxidation rates exhibited a more gradual trend of decreasing activity. These results suggest that Gulf-wide circulation patterns dispersed and redistributed methanotrophic biomass that bloomed and accumulated in the wake of the Deepwater Horizon blowout, and that this biomass was able to perpetuate elevated methanotrophic activity for multiple years after the blowout at levels above anticipated background rates. This dataset provides a rare view of the response of an ocean ecosystem to a large pulse of methane and reveals unanticipated dynamics of microbial methanotrophy as a result of such human-induced methane releases.

Keywords: Deepwater Horizon; Gulf of Mexico; Methane oxidation; Methane; Water column

1. Introduction

Methane, a potent greenhouse gas that has a global warming potential 28 times that of carbon dioxide, influences Earth's climate through its impact on the atmospheric infrared radiation balance (IPCC 2013; Nauw et al., 2015). The ocean is a net source of methane to the atmosphere (~10 Tg yr^{-1}). This methane is derived from a mix of biogenic (methanogenesis) and thermogenic sources via a number of processes, including the destabilization of gas hydrates (Bernard et al., 1976; Reeburgh, 2007). The majority of the methane introduced into the oceanic environment is consumed through methane oxidation within sediments and in the water column. Sedimentary anaerobic oxidation of methane (AOM) is the primary sink of methane in the ocean, but aerobic methane oxidation plays an important role in maintaining low background methane concentrations in most of the ocean even when methane escapes the sedimentary biofilter (Reeburgh, 2007; Knittel and Boetius, 2009).

* Department of Marine Sciences, University of Georgia, Athens, GA, US

† School of Earth and Atmospheric Sciences, Georgia Institute of Technology, Atlanta, GA, US

Corresponding author: Samantha B. Joye (mjoye@uga.edu)

The Gulf of Mexico is a unique ecosystem where liquid (oil) and gaseous (methane and other alkanes) hydrocarbons reside naturally in deep subsurface reservoirs that discharge slowly and diffusely at the seabed (Kennicutt et al., 1988; Roberts et al., 1999). Salt diapirism generates fault networks that facilitate discharge of oil, gas, and brine from these reservoirs through the sediments and eventually into the overlying water column (Kennicutt et al., 1988; Roberts and Carney, 1997). At some seeps, brine is discharged concomitantly with oil and gas. The high salinity of brine can impede the formation of methane hydrates, which may increase the methane flux into the water column (Wilson and Ruppel, 2007). To date, at least 22,000 natural seeps have been identified; 914 generate oil slicks that are visible from space (http://1.usa.gov/1aKybyq; Joye et al., 2014; MacDonald et al., 2015). At one Gulf brine pool, the diffusive flux of methane was 1.1 mol m^{-2} y^{-1} (Wankel et al., 2010). Methane fluxes from a gas vent at Hydrate Ridge on the Cascadia margin off the coast of Oregon ranged from 11 to 33 mol m^{-2} y^{-1} (Torres et al., 2002). These fluxes underscore the importance of natural seeps as a source of methane to the overlying water column, and potentially to the atmosphere.

The Gulf of Mexico is significantly impacted by oil and gas exploration. Currently there are 2,024 platforms and 53,068 wells drilled at water depths ranging between 0 and >1000 m. Most active leases lie at water depths >1000 m (BOEM 2017; https://www.data.boem.gov). On April 20, 2010, the Deepwater Horizon (DWH) drilling platform suffered an uncontrolled blowout and caught fire; the rig sank on April 22, 2010, in the Mississippi Canyon area of the northern Gulf of Mexico. Sinking of the platform severed the riser, leading to the uncontrolled discharge of oil and gas into the deep water column. The well was capped 84 days later, in mid-July, after some 5,000,000 barrels of oil and 250,000 metric tonnes of low molecular weight alkane gases, mainly methane, were discharged into the Gulf ecosystem, representing a large and abrupt ecosystem perturbation (Joye, 2015; Joye et al., 2016).

The discharged low molecular weight alkane gases dissolved at depth, forming a lateral, deep-water plume (**Figure 1**) between 1,000 to 1,200 m water depth; peak methane concentrations of >380 μM in May 2010 were observed around 1,100 m (Joye et al., 2011; Joye, 2015). Solution and focusing of these gases in the deep-water plume was facilitated by the high pressures and low temperature (100–150 bar and 4–6°C; Reddy et al., 2012) combined with the presence of suspended gas hydrates at this depth in the water column (Joye et al., 2011). The increase in methane concentrations in the deep-water plume stimulated aerobic methane oxidation, which peaked at rates of 5,900 nM d^{-1} in late May/early June, about a month after the discharge began (Crespo-Medina et al., 2014). This rate is the highest reported for the oceanic water column to date and among the highest reported for an aquatic ecosystem.

The deep-water methane anomaly was concentrated in a narrow lateral plume for the first two months of the incident. Peak plume concentrations were 10^2 to 10^4 times greater than the background methane concentration in the Gulf (Joye et al., 2011). The deep-water hydrocarbon

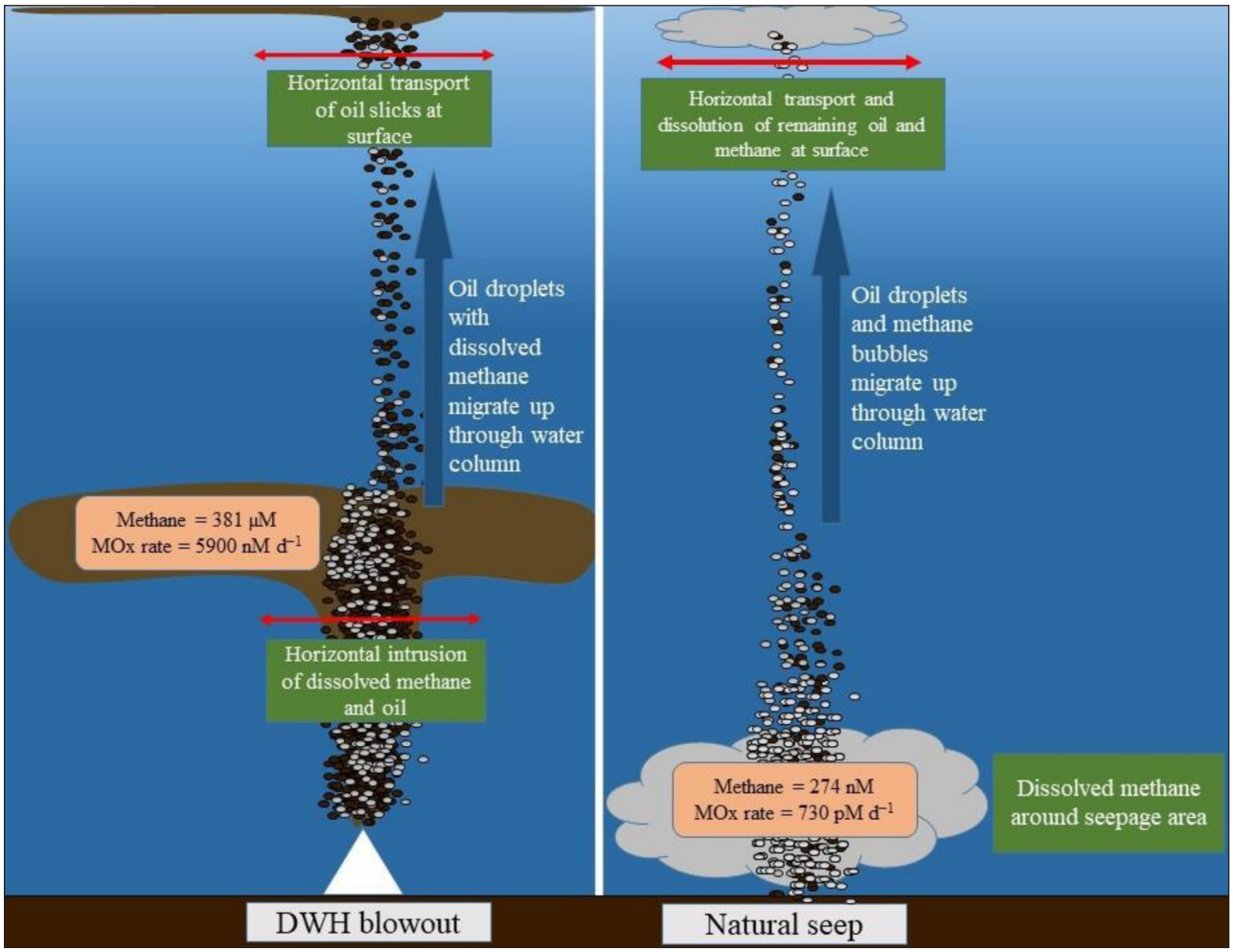

Figure 1: Anthropogenic oil and gas input versus natural seepage. Schematic depicting differences between the lateral plume created during the DeepWater Horizon disaster and the more diffuse methane-rich area created from natural seeps. Methane concentrations and MOx rates were high in the deep-water plume created during the DWH disaster. The oil and methane not trapped in the deep-water plume migrated to the surface, where surface slicks formed. At natural seepage locations, methane concentrations are elevated. Bubbles of methane and oil droplets that did not dissolve at the source, migrate through the water column and continue to dissolve until they reach the surface. MOx indicates methane oxidation rate; MOx rates and methane concentrations are from this study and Crespo-Medina et al. (2014). DOI: https://doi.org/10.1525/elementa.332.f1

plume was unique due to the large amount of dissolved methane contained within the layer and because of the extent of its multi-month duration. By July, methane had been mixed, to a various extent, through the water column.

The DWH deep-water methane-rich plume differed substantially from the dissolved methane regimes observed typically at natural seeps, which are largely controlled by bubble/hydrate interactions within the water column and site-specific physical dynamics (**Figure 1**; Leifer and MacDonald, 2003; Leifer et al., 2009; Solomon et al., 2009). The lateral scale (>20 nautical miles or >37 km) of the deep-water plume that formed in the aftermath of the DWH disaster was much larger than the dissolved methane plumes found near natural seeps. Observations made at natural seeps over the past 20 years in the Gulf of Mexico suggest that the horizontal footprint of a gas vent along the seabed is typically >1 m but <10s of m, and the vertical extent of the discharge vent is limited to several hundred meters. The DWH event represented a perturbation that is quite distinct from natural seepage regimes and offered an opportunity to study how a microbial community responds to such a large perturbation.

We present results focused on the 5-year period following the DWH discharge but also including background data from years before the DWH incident. We define a natural seep as a location within a lease block (i.e., a geographic area used for leasing and development within the Outer Continental Shelf of the northern Gulf of Mexico) where there is active gas release/seepage. Even within an area known for active seepage, there can be non-seep locations if seepage is absent in those areas. We investigated methane concentrations, methane oxidation rates, hydrography, and nutrient availability in the water column of the Gulf of Mexico each summer (2010–2015), but more frequently in 2010 and in the immediate aftermath of the blowout. This time-series data set permitted assessment of the response and recovery of the Gulf microbial ecosystem following the DWH blowout and provided opportunities for discovery that routine monitoring of a natural seep site would not provide. Methanotrophic activity – and presumably methanotroph biomass – was highest in the immediate aftermath of the DWH methane infusion, and this methanotrophic potential then dispersed throughout the water column and across the basin, sustaining elevated rate constants for three years following the blowout. This data set thus documents an unexpected long-term impact of the DWH incident on the pelagic microbial ecosystem.

2. Materials and Methods

2.1. Site description

A total of ~900 water column methane oxidation rate samples from 149 CTD casts at 31 different sites were collected during nine research cruises to the Gulf of Mexico, onboard the R/V *Pelican*, 5–15 May 2010; R/V *Walton Smith*, 25 May–6 June 2010; R/V *Endeavor*, 2–13 July 2011 (EN 496–post spill monitoring cruise), 27 June–4 July 2012 (EN510), 20 June–22 July 2013 (EN 527/528), and 29 May–20 June 2015 (EN 559); and R/V *Atlantis*, 31 March–14 April 2014 (AT26-13). Data from 2001 and 2006 were collected during expeditions of the R/V *Edwin Link* (2001, "Gulf Extreme Environments") and R/V *Atlantis* (2006, "Expedition to the Deep Slope"). The 2010 data set, originally presented in Crespo-Medina et al. (2014), is provided here as foundation for the time-series data set. Distribution of the study sites across the Gulf of Mexico is depicted in **Figure 2**; their specific names and locations are provided in Table S1.

2.2. Sample collection

A CTD-Niskin rosette system was used to obtain hydrographic profiles through the water column; Niskin bottles were triggered at specific depths based on hydrographic signatures (Figure S1). Upon recovery, each Niskin bottle was sub-sampled to determine concentrations of

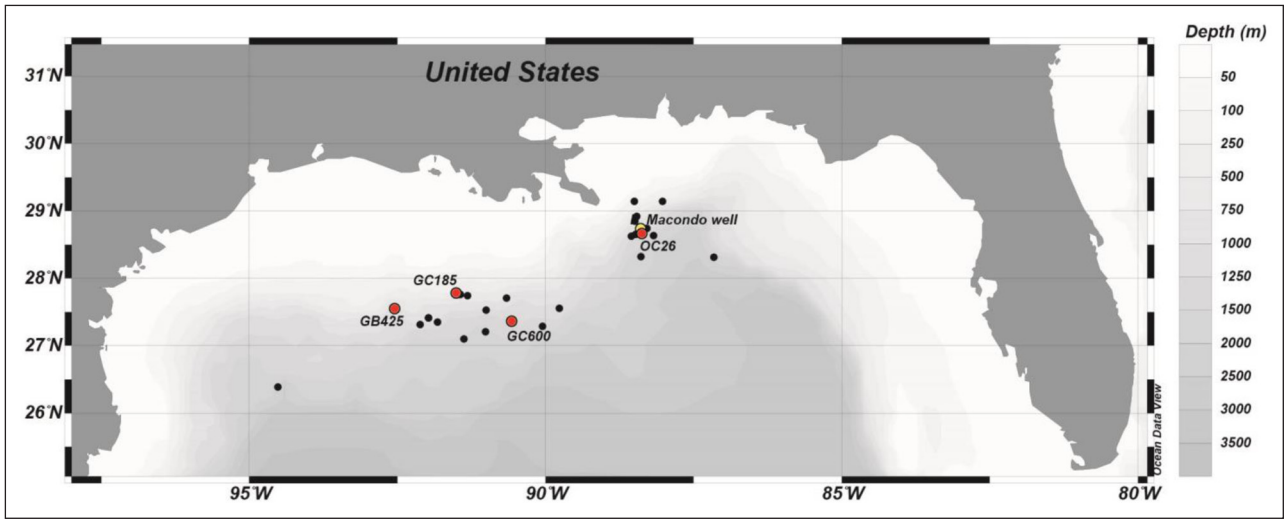

Figure 2: Distribution of sampling sites across the northern Gulf of Mexico. Sites highlighted for specific reasons in the text are identified by station designation (see Table S1). The Macondo wellhead location is denoted by the yellow point; GB425 (mud volcano), GC185, GC600, and OC26 locations are denoted by the red points. DOI: https://doi.org/10.1525/elementa.332.f2

dissolved gases and nutrients and rates of methane oxidation. Samples for dissolved methane concentrations were collected first. A 1-L PETG bottle was filled using silicon tubing, which was inserted into the bottle to allow for filling from the bottom. The PETG bottles were allowed to overflow to ensure that the water sample had minimal atmospheric exposure. Once filled, these bottles were capped headspace-free. Following collection of the methane sample, an additional 1-L PETG bottle was filled with water for use in assays of methane oxidation rate and capped headspace-free. Once the bottle for rate assays was filled, a 250-mL PETG bottle was filled with water for use in dissolved nutrient analyses and capped headspace-free. All bottles were immediately stored at 4°C until methane extraction or nutrient subsampling, which commenced within 6 hours of collection. PETG bottles for methane oxidation rates were subsampled and injected within two hours of collection during the 2011–2015 expeditions.

2.3. Multibeam echosounder surveys (MBES)

Multibeam echosounder surveys (MBES) were conducted using Kongsberg Maritime EM302 30 kHz or EM710 70 kHz MBES systems to document the location and nature of naturally occurring gas vents. A shipboard system was used during one of the cruises listed above, the R/V *Atlantis* in 2014 (R2R Program, 2013; UNOLS R2R, 2014), while during two other earlier (2012) expeditions, MBES were conducted using a remotely operated vehicle (ROV) from the R/V *Okeanos Explorer* (ROV Little Hercules; NOAA Office of Ocean Exploration and Research, 2012; NOAA, 2012) and R/V *Falkor* (ROV MK3; R2R Program, 2012; UNOLS R2R, 2012). Fledermaus GeoCoder was used to process backscatter data, and image mosaics were generated using ArcGIS (https://bit.ly/2Qn1vXD).

2.4. Methane concentrations

Methane gas was extracted from 0.8 L of seawater using a sonication/vacuum extraction technique (Schmitt et al., 1991; Lammers and Suess, 1994). A subsample of the recovered gas (0.5–1.0 mL) was injected into a gas chromatograph (model 8610C, SRI® Torrance, California) outfitted with a HaySepD packed column and a flame ionization detector. The methane concentration was calculated by comparing sample areas to areas determined from high purity methane standards (Scott Specialty Gases®); the detection limit was 0.5 nM methane.

2.5. Methane oxidation rates

Microbially mediated rates of aerobic methane oxidation were determined by tracking the conversion of methane-derived tritium into the product, tritiated water (Equation 1). Tritiated methane (C^3H_4) has a high specific activity (0.7 TBq/mmol). Despite addition of high activity (~33 kBq as a gas bubble), the maximal addition of methane was ~2 nM, which would at most double the *in situ* pool when concentrations were in the low nM range.

$$C^3H_4 + 2O_2 \rightarrow CO_2 + 2\,{}^3H - H_2O \quad \text{(Eq. 1)}$$

An open-bore 60-mL syringe fitted with silicon tubing was used to pull sample from the bottom of the PETG bottle, ensuring that any millimeter-sized aggregations of methanotrophic biomass were not excluded. Sample aliquots were distributed into 16-mL Hungate tubes and capped headspace-free using Labco® septa and a screw cap. At each depth, rate assays were performed in triplicate, with one killed control. Killed controls were amended with 37% formaldehyde to halt microbial activity prior to tracer addition. The tritiated methane tracer was injected as dissolved gas in 100 µL (2011–2014) or as a gas bubble in 20 µL (2015); in both cases, the final aqueous-phase tracer activity, quantified in sub-samples after incubation, was ~20 kBq (Sandbeck and Reeburgh., 1989; Valentine et al., 2001; Carini et al., 2005). Samples were incubated at *in situ* temperature (4, 8, 12, or 20°C) in shipboard incubators inside radiation isotope isolation vans except for the May–June 2010 samples, which were incubated onshore after the expedition (see Crespo-Medina et al., 2014, for details).

After an incubation period of 48–60 hours, the production of tritiated water was quantified as follows. Reactions were terminated by emptying the content of each Hungate tube into a 20-mL scintillation vial containing 2 mL of 37% formaldehyde. For at least one sample from each set, a 100 µL sub-sample was collected immediately after opening, but prior to termination, to verify the total $^3H–CH_4$ activity added to the sample. The radioactivity of this sample was quantified on a scintillation counter by injecting the sub-sample into a vial containing Scintillation cocktail (ScintiSafe Gel®). For the other samples, immediately following termination of microbial activity, labeled $^3H–CH_4$ was removed by purging the sample with hydrated air for at least 45 minutes. Scintillation cocktail was added to an aliquot of the sample at a ratio of 1:5 sample:scintillation cocktail, which was the optimal ratio for minimizing chemiluminescence. The activity of $^3H–H_2O$ was quantified using a Beckman® 6500 liquid scintillation counter. Methane oxidation rates were calculated by multiplying the fractional turnover rate constant, k (d^{-1}), by the CH_4 concentration (nM) measured from the water sampled at each specific location (Equations 2 and 3). The detection limit for methane oxidation rate (MOx) was 0.5 pmol L^{-1} d^{-1}.

$$k = \left[\mathrm{DPM} - {}^3H_2O / \left(\mathrm{DPM} - {}^3H_2O + \mathrm{DPM} - C^3H_4\right)\right] / \mathrm{time} \quad \text{(Eq. 2)}$$

$$\mathrm{MOx} = k\left[CH_4\right] \quad \text{(Eq. 3)}$$

In Equation 2, DPM–^3H_2O is the activity in the oxidation product, DPM–^3H_2O + DPM–C^3H_4 is the total activity of tritiated methane, and 'time' is the incubation time in hours.

2.6. Nutrient concentrations

Nutrient samples were collected directly into 250-mL PETG bottles from the CTD as described previously. Next, a subsample was filtered through a 0.22-µm Target® filter into a 60-mL HDPE bottle. These bottles were sub-sampled for ammonium (5 mL) which was preserved with phenol and

run onboard the ship using the standard phenol hypochlorite colorimetric method and a HACH spectrophotometer with a minimum detection limit of 0.1 μM (Solorzano, 1969). ACS reagent grade NH_4Cl was used to generate the standard curve. After sampling for ammonium, the HDPE bottles were immediately frozen at –20°C to preserve other constituents until analysis, which occurred within 6 months of collection. NO_x (nitrate + nitrite), nitrite, and phosphate concentrations were measured using a Latchat Instruments FIA 8000 Autoanalyzer and standard protocols 31-107-04-1-A (for NO_x and nitrite; Diamond, 1997) and 31-115-01-1-H (phosphate; Knepel and Bogren, 2002), with detection limits of 0.7 μM and 0.16 μM, respectively. The methods were standardized by comparison to a range of ACS reagent grade KNO_3, KH_2PO_4, and $NaNO_2$ solutions treated identically to samples. Nitrate concentrations were calculated as the difference between NO_x and nitrite.

Total dissolved nitrogen (TDN) was determined by subjecting filtered seawater samples to high temperature catalytic oxidation on a Shimadzu Instruments TOC-V coupled to a Shimadzu Instruments Total Nitrogen unit; the detection limit was 0.4 μM. The method was standardized by comparison to a range of KNO_3 and glycine solutions treated identically to the seawater samples. Ammonium concentrations were determined again in samples following storage using the phenol hypochlorite method (to obtain a robust ammonium value for the TDN calculation) and analyzed on the Shimadzu Instruments Spectrophotometer Model UV-1601 (Solorzano, 1969). This ammonium value, along with NO_x, was used to calculate the dissolved organic nitrogen (DON) concentration as the difference between TDN and dissolved inorganic N (NO_x + ammonium). Total dissolved phosphorus (TDP) was determined via high temperature combustion and hydrolysis of filtered samples and analyzed on the Shimadzu Instruments Spectrophotometer Model UV-1601 with a minimum detection limit of 0.2 μM (Solorzano and Sharp, 1980; Monaghan and Ruttenberg, 1999); ACS reagent grade potassium orthophosphate was used to generate a standard curve. Dissolved organic phosphorus (DOP) was calculated as the difference between TDP and inorganic phosphate.

2.7. Data analysis and statistics

Some of the study sites were known to be natural hydrocarbon seeps, while others were 'control' sites not known for seepage. Natural seep samples were classified as 'seepage' or 'non-seepage' based on the bottom-water methane concentration: seepage ≥10 nM CH_4 and non-seepage <10 nM CH_4. This designated threshold was roughly 6-fold higher than the median background methane concentration, 1.7 nM (Solomon et al., 2009; and data presented herein). A two-way analysis of variance was performed on each year of the data set to assess the effects of year and classification (seepage or non-seepage). As only three depth profiles were available between 2001 and 2006, they were not included in this analysis. Comparison of means (Steel Dwass test) was performed on the methane concentrations to assess the differences between years. Kendall's Tau correlation analysis was used to determine strength of relationship between variables.

Nitrate, DON, phosphate, and DOP concentrations from 2010, 2012, 2013, 2014, and 2015 from GC600 and OC26 were binned based on the depth (400 m and above, between 400 and 1000 m, or 1000 m and below). These water depths were chosen to delineate the DWH deep-water methane plume and the methane anomaly associated with the deep chlorophyll maximum (Joye SB, personal observation). Ammonium was not included in these analyses because the majority of the values were below detection. Comparison of means (Steel Dwass) was performed on the nutrient concentrations to assess the differences between years. Kendall's Tau correlation analysis was used to determine if there was a relationship between methane concentration, rate constant, and nutrient concentrations. All statistical analyses were performed using JMP® Pro 13.

3. Results

3.1. Multibeam surveys of natural seepage

The MBES data collected and processed during 2012 and 2014 were used to identify locations of natural hydrocarbon and methane seepage. Two major seep sites, GC185 and GC600, and one non-seep site, OC26, close to the Macondo wellhead, are highlighted here (**Figure 3**). GC185 is a shallow cold seep (water depth of ~500 m) where dissolved alkane gases and oil discharge into the water column (**Figure 3A**). GC600 is a cold seep that lies at greater depth (1200 m) and supports two distinct seepage fields, called Megaplume and Birthday Candles; these vents discharge oil and dissolved alkane gases, mainly methane, into the overlying water column (**Figure 3B**). Both GC185 and GC600 release significant amounts of methane from the seabed leading to super-saturation throughout the water column.

3.2. Spatio-temporal trends in methane dynamics

We evaluated methane dynamics in 2001, 2006, and 2010 (Deepwater Horizon blowout) through 2015 to document spatial and temporal trends in Gulf of Mexico pelagic waters (**Figure 4**). At natural seeps prior to the DWH blowout (in 2006), methane concentrations as high as 37 μM were observed, for example, within the vertical plume emanating naturally from an active mud volcano (GB425). At natural hydrocarbon seeps, vertical structure dominated the methane profile, and concentrations ranged typically from 10 to 250 nM, with the highest concentrations observed at the seabed near the source (**Figure 5**). Another increase in concentration was observed near the top of the pycnocline, and sometimes a third peak was associated with the deep chlorophyll maximum (Joye SB, personal observations). In contrast to the range of methane concentration profiles observed at natural seeps, samples collected during the DWH blowout exhibited both vertical and horizontal structure, with highest concentrations well above the seabed in the deep-water plume and significant anomalies occurring above and below the plume (**Figures 1** and **5C**).

Methane concentrations ranged from 0.8 to 274 nM in 2001 for pre-blowout conditions and from below detection to 381 μM for blowout and post-blowout conditions.

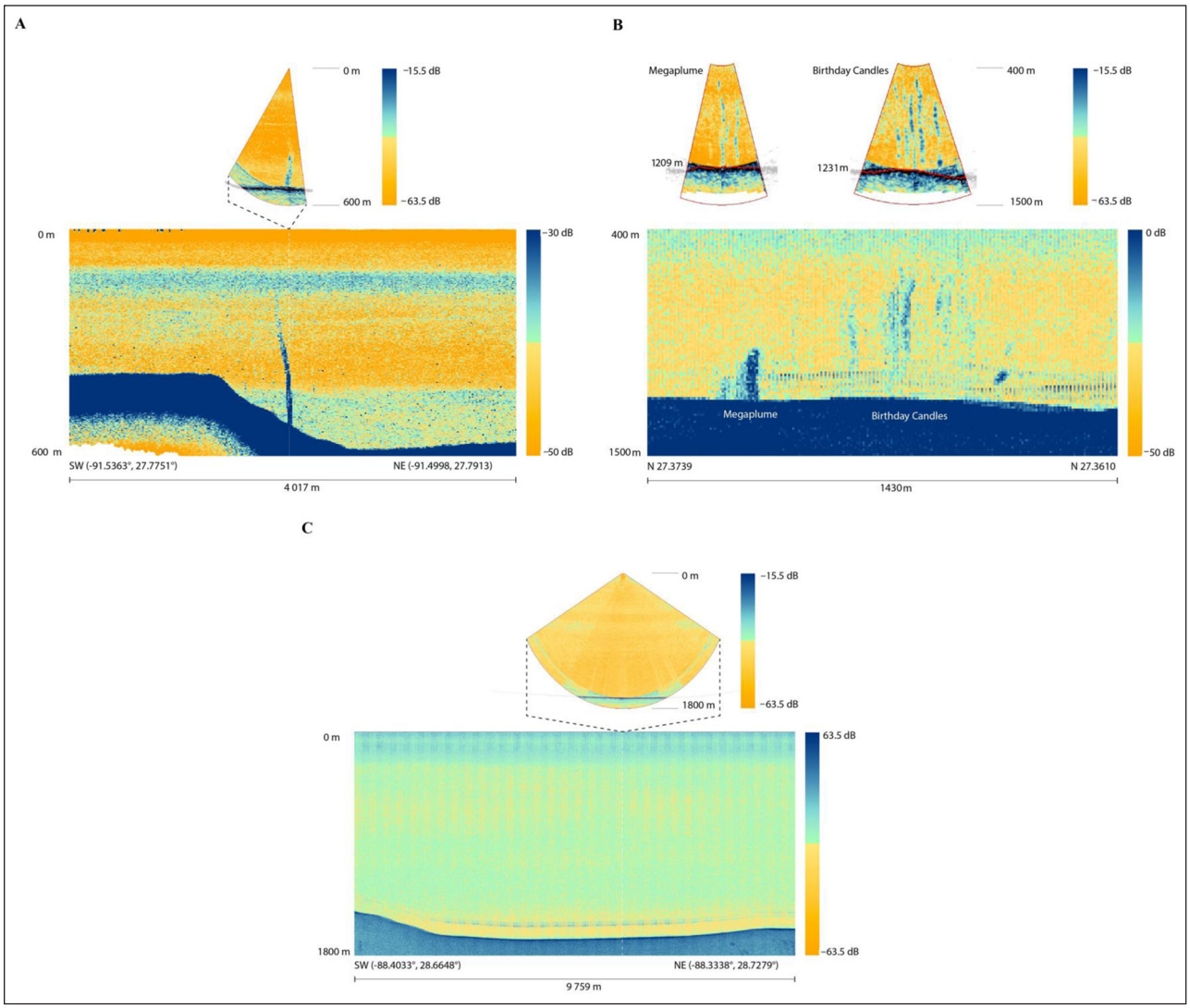

Figure 3: Multibeam echosounder surveys at three sites. Gas plumes detected at GC185 **(A)** and GC600 **(B)** and absence of seepage at OC26 **(C)** using multibeam surveys during the 2012 R/V *Okeanos* and *Falkor* expeditions and the 2014 R/V *Atlantis* cruise. Multiple seeps are apparent in the multibeam data for GC600. These seeps are associated with salt-driven tectonics in the Gulf of Mexico. DOI: https://doi.org/10.1525/elementa.332.f3

The highest concentrations were observed in 2010 (DWH blowout) and the lowest concentrations were observed in 2013 and 2015. Seep sites had elevated methane concentrations compared to non-seep areas. The methane concentrations across the study area were significantly higher in 2010 due to the DWH blowout (n = 87–201; $p < 0.0001$; Steel Dwass mean comparison), and particularly high in areas within 30–50 nautical miles of the wellhead (GRIIDC DOI: https://doi.org/10.7266/N7KK98T1; Crespo-Medina et al., 2014). After 2010, methane concentrations decreased post-blowout for all locations examined (**Figure 4A**).

Methane oxidation rates ranged from below detection (0.5 pmol L^{-1} d^{-1}) to 730 pmol L^{-1} d^{-1} for pre-blowout conditions, and from near the detection limit to 5900 nmol L^{-1} d^{-1} for blowout and post-blowout conditions. The highest rates were measured in 2010 (DWH blowout), followed by 2011 and 2012, and lowest rates were documented in 2015 (**Figure 4B**). The rate constant for methane oxidation ranged from 1.4×10^{-6} to 0.12 d^{-1}, with the highest values observed in 2010, 2011 and 2012 and the lowest observed in 2001, 2006, and 2015. The rate constant for both seep and non-seep sites increased during the DWH blowout and remained elevated above background until 2013, when the rate constant decreased to near pre-blowout conditions (**Figure 4C**). Depth profiles of methane concentration, methane oxidation rate, and rate constant at GC600 (seep site) and OC26 (near wellhead, no active seepage) are depicted in **Figure 6**. GC600 as a natural seep site supported much higher methane concentrations, methane oxidation rates, and rate constants (**Figure 6A–C**), compared to the OC26 site (**Figure 6D–F**).

A two-way ANOVA showed that methane concentrations differed significantly between years and between classifications (seep vs. non-seep), and that there was a significant interaction between year and classification. Methane oxidation rates followed a similar statistical pattern, with significant differences between years and classifications, and interaction between the two variables. The rate constant was significantly different only between years (**Table 1**).

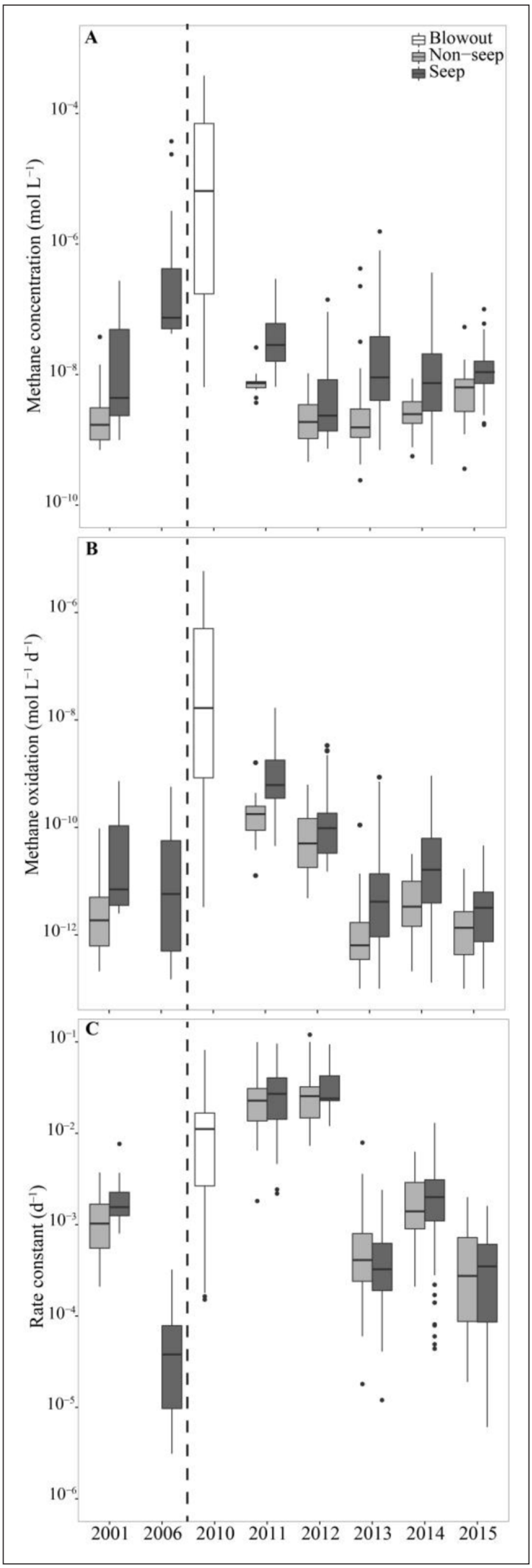

Figure 4: Box plots of non-seep and seep locations Gulf of Mexico sites compared to DWH blowout conditions. (A) Methane concentration (mol L^{-1}), **(B)** methane oxidation rate (mol L^{-1} d^{-1}), and **(C)** rate constant (d^{-1}). The line within the box is the median, and the boundary of the boxes indicates the 25th and 75th percentiles. Error bars above and below indicate the 90th and 10th percentiles. Filled circles represent outliers. N values are (non-seep and seep) 22 and 20 for 2001; 11 and 76 for 2011; 56 and 32 for 2012; 101 and 90 for 2013; 45 and 116 for 2014; 68 and 61 for 2015; 17 for mud volcano conditions at GB425 in 2006; and 81 for blowout conditions in 2010. The 2010 blowout box includes all data from all sites (non-seep and seep) during the blowout year, as reported by Crespo-Medina et al. (2014). Dashed line separates background conditions prior to the DWH blowout. Note the log scale for A and B. DOI: https://doi.org/10.1525/elementa.332.f4

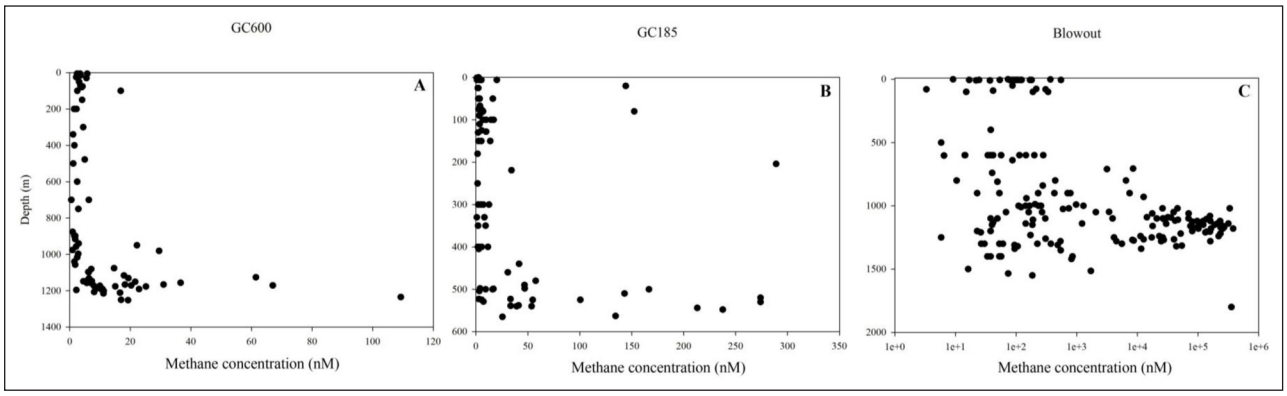

Figure 5: Depth profiles of methane seepage at natural seep sites compared to the DWH blowout profile. Methane concentrations are shown with depth for natural seep sites GC600 **(A)** and GC185 **(B)** and for the DWH blowout site **(C)**. Concentrations for the blowout site are as reported by Crespo-Median et al. (2014). DOI: https://doi.org/10.1525/elementa.332.f5

Table 1: The *p*-values of analysis of variance showing the effects of year, site classification, and their interaction on each response variable. DOI: https://doi.org/10.1525/elementa.332.t1

Response variable	Year	Classification	Interaction
Methane concentration	<0.0001*[a]	<0.0001*	0.0002*
Methane oxidation	<0.0001*	<0.0001*	0.0284*
Rate constant	<0.0001*	0.67	0.8

[a] Asterisks indicate significant effect at 5% significance level.

3.3. Macronutrients

We investigated nitrate, DON, DOP, and phosphate concentrations in 2010 at the DWH impacted locations and in 2012, 2013, 2014, and 2015 at long-term monitoring locations (OC26 and GC600). Nitrate concentrations at OC26 and GC600 ranged from below detection to 36 μM, and DON concentrations ranged from below detection to 12 μM. Phosphate concentrations at OC26 and GC600 ranged from below detection to 2 μM, and DOP concentrations ranged from below detection to 1 μM. Nutrient concentrations exhibited no marked interannual variability. Depth profiles of nutrients are shown in **Figure 7**.

Nutrient concentrations in the water column were binned (400 m and above, between 400 m and 1000 m, and 1000 m and below) in order to capture the distinct methane regimes typically found within the water column of the Gulf of Mexico. Results from the comparison of means performed on the OC26 and GC600 data are provided in Table S2. Additional results from the Kendall's Tau analysis of the correlation between nutrient concentrations and methane oxidation rates and rate constant are shown in Tables S3–S5.

4. Discussion

4.1. Overview of deep water impacts and pre-blowout conditions

The goal of this study was to compare patterns of methane dynamics in the northern Gulf of Mexico before, during, and after the DWH blowout. As such, we investigated spatial and temporal patterns of methane concentration, oxidation rate, and rate constant in the northern Gulf water column. A significant but ephemeral increase in methane oxidation activity in response to the methane input from the DWH blowout was reported by Crespo-Medina et al. (2014). However, the long-term response of the methane infusion on the activity of Gulf methanotrophic populations, as well as patterns of methane oxidation before the incident have not been described. Determining the magnitude and dynamics of the response to the DWH blowout and the recovery of the pelagic methanotrophic community in the Gulf of Mexico following the DWH methane injection is critical for understanding how ecosystem-scale methane cycling is influenced by pulsed high methane loads. This data set, derived from ~900 discrete measurements of methane concentration, oxidation rate, and rate constant from 149 CTD casts made in 2001, 2006, and 2010 through 2015, represents the most extensive compilation of data on methane dynamics for a pelagic ocean ecosystem.

The data presented here support the following conclusions:

I. Widespread elevations in methane oxidation rates measured across the northern Gulf in the wake of the BP Deepwater Horizon blowout indicate the dispersion of active methanotrophic biomass away from the point source of methane injection (i.e., the Macondo wellhead).
II. The DWH blowout led to a relatively short-term bloom of methanotrophs in the methane-enriched deep water (Crespo-Medina et al., 2014), but potential rates of methanotrophic activity re-

mained elevated in the region for several years, despite the fact that methane concentrations approached background after 2010. Methane oxidation rates retreated toward pre-blowout levels more slowly than methane concentrations.

III. Basin-wide circulation dispersed the residual methane from the DWH blowout as well as the biomass produced. This dispersed methanotrophic population accounted for the sustained elevated rate constants observed for multiple years post-blowout.

Prior to the DWH blowout, in 2006, methane oxidation rates measured in Gulf waters were relatively low, even in the seepage field of the GB425 mud volcano where methane concentrations were as high as 37 μM (**Figure 4**). Although mud volcanoes expel large amounts of methane, discharge is periodic and high flux events are typically short-lived (MacDonald et al., 2000). Highly eruptive periods are often followed by periods of either weak or no discharge activity (Dimitrov, 2002). Methane oxidation in such environments is likely limited by methanotrophic biomass and the extent to which that biomass comes into contact with methane. Thus, we posit that the methanotrophic communities in waters around the GB425 mud volcano were unable to respond due to a short duration of active methane discharge and thus limited amount of time that methane concentrations were above background. Overall, unlike the DWH blowout, where oil and gas infusions led to the formation of a pronounced, methane-enriched, deep-water lateral plume that persisted for nearly two months (**Figure 1**; Joye et al., 2014), methane concentrations at the mud volcano site (GB425) were elevated only near the source of fluid release and attenuated rapidly towards the ocean surface.

In contrast to high-intensity, short-duration mud volcanoes, natural seeps are characterized by long-term diffusive flow over large spatial scales, punctuated by lower intensity (compared to mud volcanoes) bubble plumes. While methane concentrations are maintained well above background levels at these sites, particularly near the seafloor, they lack the discharge intensity to generate a deep-water methane plume such as that observed after the DWH event. As such, natural seeps are not characterized by lateral, deep-water plumes (**Figure 1**; Leifer and MacDonald, 2003; Leifer et al., 2009; Solomon et al., 2009).

The high-intensity DWH discharge produced a lateral, deep-water plume due to the presence of oily gas hydrate at depth (Joye et al., 2011) and the sublimation of this hydrate, which likely concentrated low molecular weight gases in the high-pressure, cold waters (**Figures 1** and **5**; Paris et al., 2012; Lindo-Atichati et al., 2016). The DWH blowout methane plume tracked the continental slope SW of the wellhead between depths of 900 and 1200 m. The extremely high methane concentrations associated with this plume, 10–10^3 times above the background levels of ~1.7 nM, peaked at ~300 μM between early May and mid-June 2010, and remained well above background for the remainder of the year (**Figures 4A, 5C**; Solomon et al., 2009; Joye et al., 2011; Crespo-Medina et al., 2014). Aerobic methane oxidizers responded to the influx of methane during the DWH discharge. This influx led to increased rates of methane oxidation from the background average of 60 ± 146 pmol L^{-1} d^{-1} (n = 59) to 5900 nmol L^{-1} d^{-1}, the highest rate recorded in the oceanic water column to date, in late May and early June 2010 (**Figure 4B**; Crespo-Medina et al., 2014). The long-term intensity of the DWH incident then allowed for the unprecedented spatial scale and temporal persistence of the DWH plume, providing the methane concentrations and time necessary for large-scale production of methanotrophic biomass.

4.2. Patterns of methane oxidation activity

The rate constant reflects the substrate-specific consumption of a chemical compound and describes the concentration-independent activity of the microorganisms that consume it. The equation for calculating methane oxidation rates (Equation 3) includes the methane concentration measured from the sampling location. Methane oxidation is a first order reaction, so higher methane concentrations would drive higher methane oxidation rates in a situation where the rate constant is the same between two different samples. The rate constant reflects the instantaneous capacity of the methanotrophic community to consume (i.e., turnover) methane and, thus, is reflective, to some extent, of the relative biomass of methanotrophs at a given location.

The results shown in **Figure 4C** indicate that methanotrophic activity and biomass, as reflected by the rate constant, responded to the massive increase in methane concentration during DWH blowout conditions quickly, and that activity remained elevated for at least two years post-blowout, i.e., from 2010 through 2012. Activity did not approach background levels until 2013. While methane oxidation rates and the rate constant were not significantly different between the seep and non-seep sites (**Figure 4B, C**), the rate constant at sites directly impacted by methane seepage (i.e., water sampled directly over vents with near-micromolar or higher methane concentrations) averaged 0.024 ± 0.02 d^{-1} (n = 4), with a maximal value of 0.05 d^{-1}. These high rate constants are comparable to those observed in the immediate aftermath of the DWH blowout.

In this extensive data set, we observed that relatively low methane concentrations (i.e., between 2 and 20 nM) usually resulted in no correlation between methane concentration and rate constant (Table S6). Some studies have reported that methane concentrations track rate constants due to increased biomass associated with high methane concentrations (i.e., in seepage areas) (Scranton and Brewer, 1978; Ward et al., 1987; Kadko et al., 1990; DeAngelis et al., 1993; Jones and Amador, 1993; Rehder et al., 1999; Valentine et al., 2001; Nauw et al., 2015). These studies addressed a wide variety of ecosystems, although the spatial scale of the sampling regions was smaller compared to the geographically expansive and long-term nature of the data set presented here. The lack of relationship between methane concentration and rate constant in this study suggests that other factors — variable circulation

patterns, nutrient dynamics within the water column, and the nature of natural methane inputs — influence methanotrophic activity as much as or more so than methane concentration.

4.3. Microbiology

A diverse assemblage of methane oxidizers responded to the DWH blowout, including some rare groups. The methanotrophs from the DWH blowout, as described by Crespo-Medina et al. (2014), included known methanotrophs (Rivers et al., 2013) as well as phylogenetically divergent organisms with unique *pmo*A gene sequences for methanotrophy, all of which increased in abundance in response to the gas injection. These results suggest that there is much to learn about the dominant methanotrophs in the oceanic environment and the genetic diversity and capacity of the methanotrophs that respond to a large pulse of methane. Generally, during the DWH blowout, *pmo*A gene abundances were higher in May and June compared to pre-spill conditions. After the well was capped, while methane was still above background levels, methane oxidation rates decreased. Potential nutrient limitation, grazing, viral lysis or dilution of methane concentration through physical mixing, which would have also dispersed the biomass that bloomed in response to the blowout as well, may have contributed to the decline of methane oxidation rates (Crespo-Medina et al. 2014; Joye et al., 2014).

Aerobic methanotrophs are relatively slow-growing compared to other microbes. In the laboratory, methanotrophic bacteria responding to an increase in methane may take anywhere from 3 to 7 days to form distinct colonies in the form of flocculent particles that resemble sarcina-like aggregates (Wise et al., 1999; Bowman, 2006). During the DWH incident, the methanotrophic community bloomed on a time scale of ~3 weeks in response to the rapid and sustained increase in methane in the area near the wellhead (Valentine et al., 2010; Joye et al., 2011; Kessler et al., 2011; Crespo-Medina et al., 2014). We posit that the resulting biomass and residual methane was then distributed throughout the northern portion of the Gulf basin by ocean circulation (see below).

Methanotrophic activity, and hence active populations of methanotrophs, were enriched not only in methane-rich deep waters, but also within the euphotic zone. Methane oxidation rates were elevated within the euphotic zone, especially in 2012 when the rate constants also remained elevated post-blowout (**Figure 6**). Methanotrophy-related gene abundances have been linked to distinct euphotic zone niches and potentially include the oxidation of nitrogen or reduced carbon (Sieburth et al., 1987; Ward et al., 1987; Mau et al., 2013; Tavormina et al., 2013). Of particular interest in euphotic zone methanotrophy are the copper-containing membrane-bound monooxygenases, a diverse family of enzymes encoded by diverse marine microorganisms and responsible for the oxidation of small

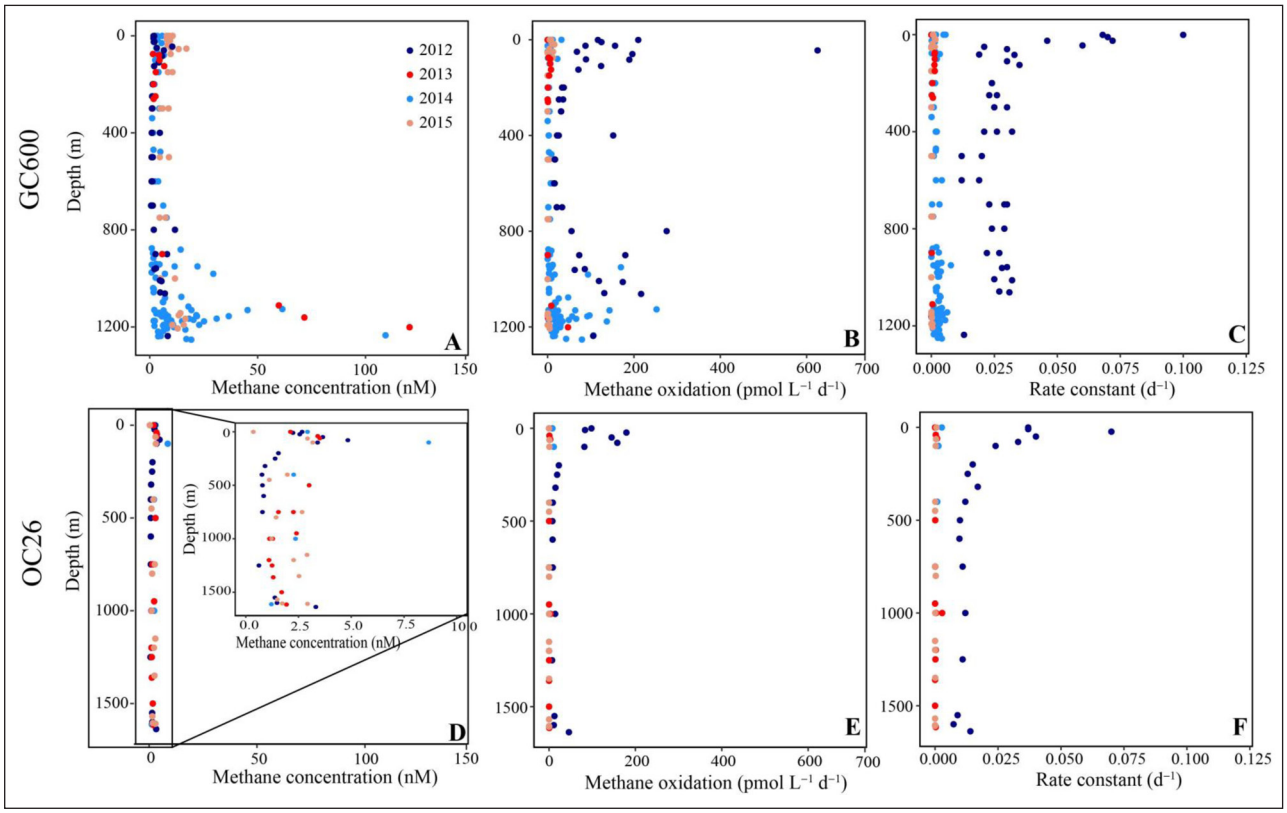

Figure 6: Methane dynamics at two distinct GOM sites. Depth profiles for the years 2012, 2013, 2014, and 2015 are shown for natural seep site GC600 **(A–C)** and non-seep site OC26 **(D–F)** for methane concentration (nM) (A and D), methane oxidation rate (pmol L^{-1} d^{-1}) (B and E), and rate constant (d^{-1}) (C and F). The inset in D provides a higher resolution scale for the low methane concentrations at the non-seep site. DOI: https://doi.org/10.1525/elementa.332.f6

reduced carbon substrates, including methane (Francis et al., 2005; Beman et al., 2010; Tavormina et al., 2013; Pedneault et al., 2014). The ubiquity of these enzymes in marine environments, especially in the euphotic zone, and the persistent methane oxidation measured in surface waters post-DWH blowout suggest that functionally plastic microorganisms may have novel implications for methane cycling in the Gulf of Mexico.

The absence of canonical methanotrophs in the euphotic zone of the Gulf of Mexico characterized by concurrent methane and chlorophyll *a* maxima was reported by Rakowski et al. (2015). They found instead that the presence of hydrocarbon degraders correlated with methane concentration in the euphotic zone. These findings suggest that oil-degrading bacteria may possess the enzymatic capacity to oxidize low molecular weight alkanes, possibly even methane (Rubin-Blum et al. 2017). Rubin-Blum et al. (2017) discovered a novel copper monooxygenase in oil-degrading *Cycloclasticus* bacteria that mediates the oxidation of propane, butane and ethane; they also determined that the methane monooxygenase genes employed by these benthic dwelling *Cycloclasticus* were very similar to those encoded by the free-living pelagic *Cycloclasticus* found in the DWH deep-water plume. While methane oxidation was not documented by Rubin-Blum et al. (2017), their results along with those of Crespo-Medina et al. (2014) raise the intriguing possibility that organisms not normally considered as methanotrophs play a role in methane oxidation in the ocean. We speculate that currently undescribed methanotrophs contributed significantly to the sustained elevations in methane oxidation activity measured in Gulf of Mexico waters in this study and are exploring that possibility.

4.4. Physical mixing

Crespo-Medina et al. (2014) observed that physical processes dispersed methane vertically throughout the water column over a time scale of several months. However, the results presented here suggest that lateral dispersion over scales not recognized at that time was also important. The mean circulation along the continental slope in the northern Gulf of Mexico is determined by the interplay of along-shore boundary currents, recirculation zones and topographic Rossby waves (Bracco et al., 2016; Liu et al., 2018). Numerical simulations with models resolving dynamics down to 1 km in the horizontal have shown that eddies and vorticity filaments at the kilometer scale are routinely formed from horizontal shear layers at the edges of highly intermittent, bottom-intensified, along-slope currents that trap material efficiently in their interior. Transport and mixing are more intense to the west of the Mississippi Fan than in De Soto Canyon (Bracco et al., 2016; Cardona et al., 2016). Physical model outputs in Bracco et al. (2016) displayed dispersion patterns in agreement with those of the deep plume in the first few weeks after the DWH blowout, as quantified by the oxygen anomalies measured between 1000 m and 1200 m, and with those followed by the fluorescent dye released near the DWH site (lease block MC297) at approximately the same depth in summer of 2012 (Ledwell et al., 2016).

Data from modeling tracer dispersion from the DWH site (Bracco et al., 2016) support the hypothesis that physical mixing dispersed methanotrophic biomass across the continental slope, helping to sustain methanotrophy for several years following the DWH explosion. The modeling experiments in Bracco et al. (2016) followed the dispersion of a tracer released at site MC297 for one year; they revealed that by the end of the integration the tracer spread across the area encompassed by the 1500-m and 2000-m isobaths where most of the data analyzed in this work were collected, but that the tracer was not uniformly distributed. About 10% of the modeled tracer remained concentrated to the immediate south and southwest of MC297 in the first year, with concentrations potentially too high to be fully consumed (see Figure 16 in Bracco et al., 2016). It is reasonable to assume that further homogenization took place in the following year, effectively injecting in a nearly continuous way sufficient methane to sustain methanotrophic microorganisms along most of the continental slope (Steinle et al., 2015, 2016).

Methane injected into the water column at seep sites, on the other hand, is subject to a different kind of mixing. Bubble plumes augment vertical mixing by rising into the overlying water column. Bubbles can rise 10–1000 m into the water column in a few days, upwelling deep, nutrient-rich waters to the ocean surface above seeps, through the added mass mechanism (Leifer and MacDonald, 2003; Greinert et al., 2006; Leifer et al., 2006; Sauter et al., 2006; Solomon et al., 2009; D'souza et al., 2016). Vertical mixing related to bubble plumes may thus replenish depleted nutrients while also transporting high activity methanotrophic biomass throughout the water column. Horizontal and vertical water mass exchange has the ability to displace, dilute or otherwise alter the extant microbial community (Wilkins et al., 2013). The upward advection through bubbles common at natural seepage locations, on the other hand, could alter and impact methane oxidation activity locally within the water column (Steinle et al., 2015). Available physical data suggest that natural seeps impact time scales on the order of 10 days, with limited lateral spreading because of the upwelling velocity of bubbles (D'Souza et al., 2016).

4.5. Nutrients

Typically, the low observed rates of methane oxidation are insufficient to impact the water column inventory of macronutrients (nitrate, DON, phosphate, and DOP). However, during periods of high methane loading, e.g., in the aftermath of the DWH blowout, increased rates of methanotrophy, as well as heterotrophic processes, in the deep-water plume (Valentine et al., 2010; Redmond and Valentine, 2012; Rivers et al., 2013; Crespo-Medina et al., 2014; Mason et al., 2014; Yang et al., 2016) depleted concentrations of nitrate and phosphate in plume waters (**Figure 7**). In the immediate wake of the blowout in 2010, significant depletion of phosphate and nitrate concentrations in deep waters near the wellhead was observed (**Figure 7**; Table S5; Shiller and Joung, 2012). At two other sites, OC26, two nautical miles south of the Macondo wellhead, and GC600, a natural seep site ~180 nautical

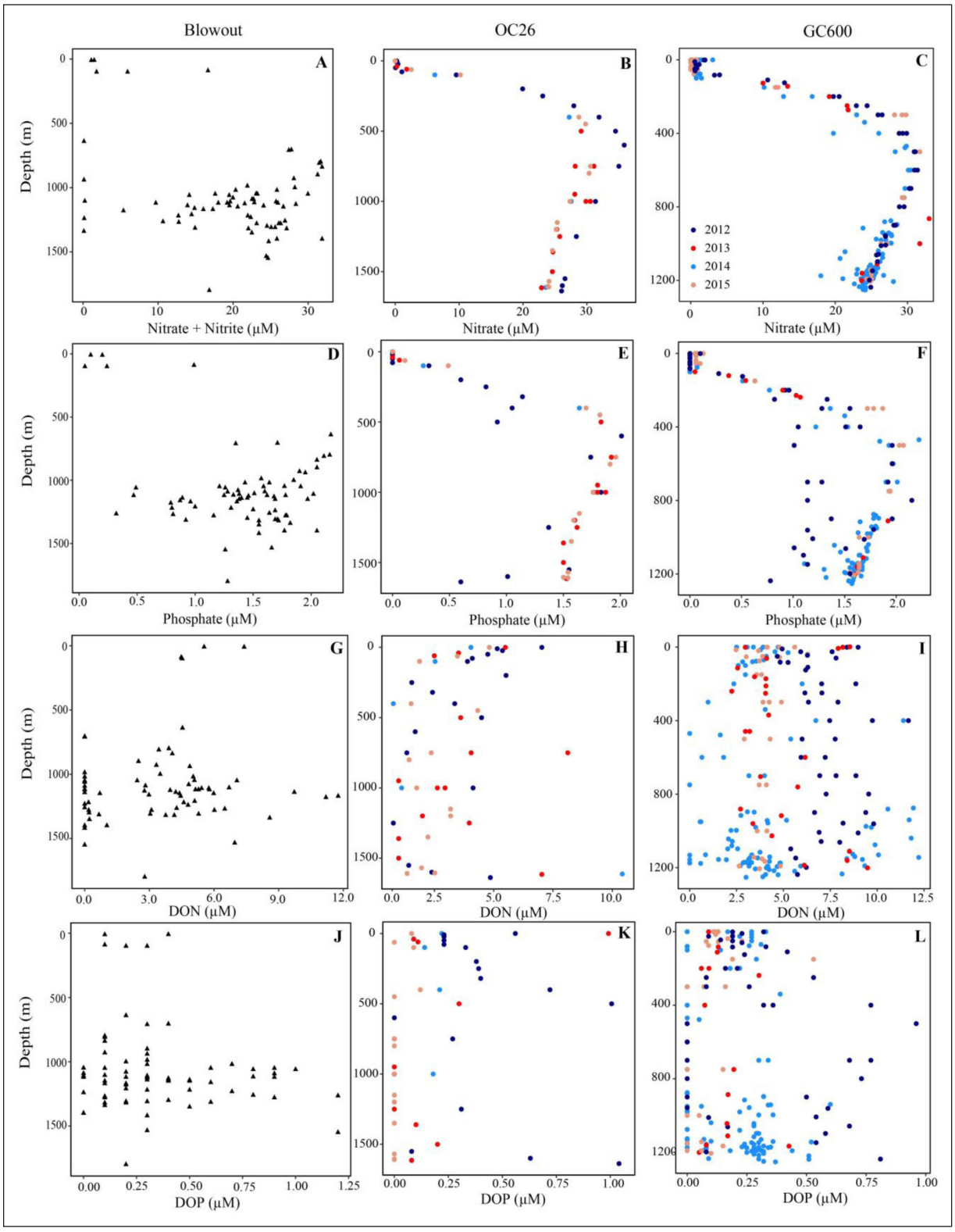

Figure 7: Nutrient characteristics at two distinct GOM sites and the DWH blowout site. Depth profiles are shown for concentrations (μM) of nitrate + nitrite or nitrate **(A–C)**, phosphate **(D–F)**, dissolved organic nitrogen **(G–I)**, and dissolved organic phosphorus **(J–L)** for the DHW blowout site in 2010 (A, D, G, J), and for non-seep site OC26 (B, E, H, K) and seep site GC600 (C, F, I, L) in 2012, 2013, 2014, and 2015. DOI: https://doi.org/10.1525/elementa.332.f7

miles to the southwest of the wellhead, water column profiles exhibited no such nutrient drawdown in 2012–2015. Other than 2010, nitrate and phosphate concentrations showed no correlation with methane oxidation rates (**Figure 7**; Table S2).

4.6. New baseline

We observed a steady decrease in methane oxidation rates following the peak in activity observed after the DWH blowout. Broad patterns of activity after 2013 were comparable, suggesting that the Gulf ecosystem may have

achieved a new baseline with respect to methane oxidation rates and methanotrophic activity. These results are critical for understanding how the marine environment responds to a large-scale perturbation, such as the DWH blowout. Using the rate constant as a proxy for methanotroph biomass, we suggest that methanotrophic biomass was dispersed basin-wide following the blowout, enhancing activity over a broad geographic area. Rate constants returned to near pre-blowout values in 2013. Although the specific ecological factors controlling methane oxidation within the Gulf of Mexico are not fully understood, it is clear that water mass movement combined with methane availability were key factors determining methane oxidation activity from 2010 to 2012 post-DWH blowout.

This extensive data set highlights the value and necessity of sustained long-term measurements for documenting microbial responses to anthropogenic perturbations. Methanotrophic bacteria responded to the DWH blowout, were distributed basin-wide, and remained active from 2010 to 2012, persisting even when methane concentrations returned to pre-blowout levels. This long-term impact of the DWH blowout on Gulf methanotrophy would not have been predicted *a priori* from studies at natural seep environments. Without this unique time-series data set, the time scale of the Macondo impact would have remained unconstrained. This study advances understanding of how microbial populations respond to large-scale methane releases and sustained exposure. Future releases are possible, if not likely, given the potential for methane hydrate destabilization in response to warming oceans and for industry-related accidental releases due to increased offshore oil and gas exploration and production. These risks make it essential to document and understand environmental baselines, underscoring the importance of long-term monitoring to assess the impacts of anthropogenic disasters and ecosystem responses to them.

Data Accessibility Statements

The data presented in this paper are publicly available through the Gulf of Mexico Research Initiative Information and Data Cooperative (GRIIDC) at https://data.gulfresearchinitiative.org (DOI: https://doi.org/10.7266/N7KK98T1, https://doi.org/10.7266/N7DV1GWK, https://doi.org/10.7266/N77M05XZ, https://doi.org/10.7266/N7KW5D1Z, https://doi.org/10.7266/N7G44N83, https://doi.org/10.7266/N7NS0RW0, https://doi.org/10.7266/N7QR4V7H).

Supplemental Files

The supplemental files for this article can be found as follows:

- **Supplementary Table 1.** Station names, Latitude, and Longitude. DOI: https://doi.org/10.1525/elementa.332.s1
- **Supplementary Table 2.** Results from comparison of means performed on nitrate and phosphate data in 2010, 2012, 2013, 2014, 2015 from OC26 and GC600. DOI: https://doi.org/10.1525/elementa.332.s1
- **Supplementary Table 3.** Kendall's Tau correlation analysis between nitrate, phosphate, methane oxidation (MOx), and turnover constant (K) in 2010, 2012, 2013, 2014, 2015 at OC26 and GC600 for 400 m and above in the water column. DOI: https://doi.org/10.1525/elementa.332.s1
- **Supplementary Table 4.** Kendall's Tau correlation analysis between nitrate, phosphate, methane oxidation (MOx), and Turnover constant (K) in 2010, 2012, 2013, 2014, 2015 at OC26 and GC600 for 400 m to 1000m in the water column. DOI: https://doi.org/10.1525/elementa.332.s1
- **Supplementary Table 5.** Kendall's Tau correlation analysis between nitrate, phosphate, methane oxidation (MOx), and Turnover constant (K) in 2010, 2012, 2013, 2014, 2015 at OC26 and GC600 for 1000 m and below in the water column. DOI: https://doi.org/10.1525/elementa.332.s1
- **Supplementary Table 6.** Kendall's Tau correlation analysis between turnover constant and methane concentration. Data was separated by turnover constant, year of sampling, and seep vs non-seep. DOI: https://doi.org/10.1525/elementa.332.s1
- **Supplementary Figure 1.** Hydrographic profiles at OC26 (a) and GC600 (b). DOI: https://doi.org/10.1525/elementa.332.s1

Acknowledgements

We thank the ship's crew and science parties of the R/V *Pelican*, R/V *Walton Smith*, R/V *Endeavor*, R/V *Edwin Link*, R/V *Atlantis*, R/V *Falkor*, and R/V *Okeanos Explorer* for assistance at sea collecting samples. We thank Joe Montoya, Ryan Sibert, and Andy Montgomery in particular for help at sea and in the laboratory. This paper is ECOGIG contribution number 517.

Funding information

This research was supported by the Gulf of Mexico Research Initiative's "Ecosystem Impacts of Oil and Gas in the Gulf" (ECOGIG-2) research consortium award, NOAA Award NA07AR4300464 to the National Institute for Undersea Science and Technology, and by National Science Foundation through grants OCE-1043225 and EF-0801741 (to SBJ).

Competing interests

The authors have no competing interests to declare.

Author contributions

SBJ designed the experiments. MKR and KSH carried out the ship-board incubations and laboratory analyses. MKR, AB, MS and SBJ analyzed the data. MKR and SBJ wrote the paper and all other co-authors provided input.

References

Beman, JM, Sachdeva, R and **Fuhrman, JA.** 2010. Population ecology of nitrifying Archaea and Bacteria in the Southern California Bight. *Environ Microbiol* **12**(5): 1282–1292. DOI: https://doi.org/10.1111/j.1462-2920.2010.02172.x

Bernard, BB, Brooks, JM and **Sackett, WM.** 1976. Natural gas seepage in the Gulf of Mexico. *Earth Planet Sci Lett* **31**: 48–54. DOI: https://doi.org/10.1016/0012-821X(76)90095-9

Bowman, J. 2006. The Methanotrophs — the families Methylococcaceae and Methylocystaceae. *The Prokaryotes* **5**: 266–289. DOI: https://doi.org/10.1007/0-387-30745-1

Bracco, A, Choi, J, Joshi, K, Luo, H and **McWilliams, JC.** 2016. Submesoscale currents in the northern Gulf of Mexico: Deep phenomena and dispersion over the continental slope. *Ocean Modell* **101**: 43–58. DOI: https://doi.org/10.1016/j.ocemod.2016.03.002

Bureau of Ocean Energy management (BOEM). 2017. Platform database of all structures in the Gulf of Mexico. (viewed on 12/19/2017) https://www.data.boem.gov.

Cardona, Y, Ruiz-Ramos, DV, Baums, IB and **Bracco, A.** 2016. Potential connectivity of coldwater black coral communities in the northern Gulf of Mexico. *PLOS ONE* **11**(5): e0156257. DOI: https://doi.org/10.1371/journal.pone.0156257

Carini, S, Bano, N, LeCleir, G and **Joye, SB.** 2005. Aerobic methane oxidation and methanotroph community composition during seasonal stratification in Mono Lake, California (USA). *Environ Microbiol* **7**(8): 1127–1138. DOI: https://doi.org/10.1111/j.1462-2920.2005.00786.x

Crespo-Medina, M, Meile, CD, Hunter, KS, Diercks, A, Asper, VL, Orphan, VJ, Tavormina, PL, Nigro, LM, Battles, JJ, Chanton, JP, Shiller, AM, Joung, D-J, Amon, RMW, Bracco, A, Montoya, JP, Villareal, TA, Wood, AM and **Joye, SB.** 2014. The rise and fall of methanotrophy following a deepwater oil-well blowout. *Nat Geosci* **7**: 423–427. DOI: https://doi.org/10.1038/ngeo2156

DeAngelis, MA, Lilley, MD, Olson, EJ and **Baross, JA.** 1993. Methane oxidation in deep-sea hydrothermal plumes of the Endeavour Segment of the Juan de Fuca Ridge. *Deep Sea Res I*, **40**(6): 1169–1186. DOI: https://doi.org/10.1016/0967-0637(93)90132-M

Diamond, DH. 1997. Determination of nitrate in brackish or seawater by flow injection analysis: QuikChem Method 31-107-04-1-A. *Methods manual. Lachat Instruments.*

Dimitrov, LI. 2002. Mud volcanoes—the most important pathway for degassing deeply buried sediments. *Earth Sci Rev* **59**: 49–76. DOI: https://doi.org/10.1016/S0012-8252(02)00069-7

D'souza, NA, Subramaniam, A, Juhl, AR, Hafez, M, Chekalyuk, A, Phan, S, Yan, B, MacDonald, IR, Weber, SC and **Montoya, JP.** 2016. Elevated surface chlorophyll associated with natural oil seeps in the Gulf of Mexico. *Nat Geosci* **9**: 1–4. DOI: https://doi.org/10.1038/ngeo2631

Francis, CA, Roberts, KJ, Beman, JM, Santoro, AE and **Oakley, BB.** 2005. Ubiquity and diversity of ammonia-oxidizing archaea in water columns and sediments of the ocean. *P Natl Acad Sci USA* **102**(41): 14683–14688. DOI: https://doi.org/10.1073/pnas.0506625102

Greinert, J, Artemov, Y, Egorov, V, De Batist, M and **McGinnis, D.** 2006. 1300-m-high rising bubbles from mud volcanoes at 2080 m in the Black Sea: Hydroacoustic characteristics and temporal variability. *Earth and Planet Sci Lett* **244**: 1–15. DOI: https://doi.org/10.1016/j.epsl.2006.02.011

IPCC. 2013. Climate Change 2013: The Physical Science Basis. *Contribution of Working Group I to the Fifth Assessment Report of the Intergovernmental Panel on Climate Change*. Cambridge; New York, NY: Cambridge University Press.

Jones, RD and **Amador, JA.** 1993. Methane and carbon monoxide production, oxidation, and turnover times in the Caribbean sea as influenced by the Orinoco River. *J Geophys Res* **98**: 2353–2359. DOI: https://doi.org/10.1029/92JC02769

Joye, SB. 2015. Deepwater Horizon, 5 years on. *Science*, **349**(6248): 592–593. DOI: https://doi.org/10.1126/science.aab4133

Joye, SB, Bracco, A, Özgökmen, TM, Chanton, JP, Grosell, M, MacDonald, IR, Cordes, EE, Montoya, JP and **Passow, U.** 2016. The Gulf of Mexico ecosystem, six years after the Macondo oil well blowout. *Deep-Sea Res Part II: Topical Studies in Oceanography* **129**: 4–19. DOI: https://doi.org/10.1016/j.dsr2.2016.04.018

Joye, SB, MacDonald, IR, Leifer, I and **Asper, V.** 2011. Magnitude and oxidation potential of hydrocarbon gases released from the BP oil well blowout. *Nat Geosci* **4**(3): 160–164. DOI: https://doi.org/10.1038/ngeo1067

Joye, SB, Teske, AP and **Kostka, JE.** 2014. Microbial dynamics following the Macondo oil well blowout across Gulf of Mexico environments. *BioScience* **64**(9): 766–777. DOI: https://doi.org/10.1093/biosci/biu121

Kadko, DC, Rosenberg, ND, Lupton, JE, Collier, RW and **Lilley, MD.** 1990. Chemical reaction rates and entrainment within the Endeavor Ridge hydrothermal plume. *Earth Planet Sci Lett* **99**: 315–335. DOI: https://doi.org/10.1016/0012-821X(90)90137-M

Kennicutt, MC, II, Brooks, JM and **Denoux, GJ.** 1988. Leakage of deep, reservoired petroleum to the near surface on the Gulf of Mexico continental slope. *Mar Chem* **24**: 39–59. DOI: https://doi.org/10.1016/0304-4203(88)90005-9

Kessler, JD, Valentine, DL, Redmond, MC, Du, M, Chan, EW, Mendes, SD, Quiroz, EW, Villanueva, CJ, Shusta, SS, Werra, LM, Yvon-Lewis, SA and **Weber, TC.** 2011. Deep Gulf of Mexico. *Science* **331**: 312–315. DOI: https://doi.org/10.1126/science.1199697

Knepel, K and **Bogren, K.** 2002. Determination of orthophosphate by flow injection analysis: QuikChem Method 31-115-01-1-H. *Methods manual. Lachat Instruments*.

Knittel, K and **Boetius, A.** 2009. Anaerobic oxidation of methane: Progress with an unknown process. *Annu*

Rev Microbiol **63**(1): 311–334. DOI: https://doi.org/10.1146/annurev.micro.61.080706.093130

Lammers, S and **Suess, E.** 1994. An improved headspace analysis method for methane in seawater. *Mar Chem* **47**(2): 115–125. DOI: https://doi.org/10.1016/0304-4203(94)90103-1

Ledwell, JR, He, R, Xue, Z, DiMarco, SF, Spencer, LJ and **Chapman, P.** 2016. Dispersion of a tracer in the deep Gulf of Mexico. *J Geophys Res: Oceans* **121**(2): 1110–1132. DOI: https://doi.org/10.1002/2015JC011405

Leifer, I, Jeuthe, H, Gjøsund, SH and **Johansen, V.** 2009. Engineered and natural marine seep, bubble-driven buoyancy flows. *J Phys Oceanogr* **39**(12): 3071–3090. DOI: https://doi.org/10.1175/2009JPO4135.1

Leifer, I, Luyendyk, BP, Boles, J and **Clark, JF.** 2006. Natural marine seepage blowout: Contribution to atmospheric methane. *Global Biogeochem Cycles* **20**(3): 1–9. DOI: https://doi.org/10.1029/2005GB002668

Leifer, I and **MacDonald, I.** 2003. Dynamics of the gas flux from shallow gas hydrate deposits: Interaction between oily hydrate bubbles and the oceanic environment. *Earth Planet Sci Lett* **210**(3–4): 411–424. DOI: https://doi.org/10.1016/S0012-821X(03)00173-0

Lindo-Atichati, D, Paris, CB, Le Hénaff, M, Schedler, M, Valladares Juárez, AG and **Müller, R.** 2016. Simulating the effects of droplet size, high-pressure biodegradation, and variable flow rate on the subsea evolution of deep plumes from the Macondo blowout. *Deep-Sea Res Part II* **129**: 301–310. DOI: https://doi.org/10.1016/j.dsr2.2014.01.011

Liu, G, Bracco, A and **Passow, U.** 2018. The influence of mesoscale and submesoscale circulation on sinking particles in the northern Gulf of Mexico. *Elementa* **6**(36). DOI: https://doi.org/10.1525/elementa.292

MacDonald, IR, Buthman, DB, Sager, WW, Peccini, MB and **Guinasso, J.** 2000. Pulsed oil discharge from a mud volcano. *Geology* **28**(10): 907–910. DOI: https://doi.org/10.1130/0091-7613(2000)28<907:PODFAM>2.0.CO;2

MacDonald, IR, Garcia-Pineda, O, Beet, A, Daneshgar Asl, S, Feng, L, Graettinger, G, French-McCay, D, Holmes, J, Hu, C, Huffer, F, Leifer, I, Muller-Karger, F, Solow, A, Silva, M and **Swayze, G.** 2015. Natural and unnatural oil slicks in the Gulf of Mexico. *J Geophys Res: Oceans* **120**(12): 8364–8380. DOI: https://doi.org/10.1002/2015JC011062

Mason, OU, Han, J, Woyke, T and **Jansson, JK.** 2014. Single-cell genomics reveals features of a *Colwellia* species that was dominant during the Deepwater Horizon oil spill. *Front Microbiol* **5**: 1–8. DOI: https://doi.org/10.3389/fmicb.2014.00332

Mau, S, Blees, J, Helmke, E, Niemann, H and **Damm, E.** 2013. Vertical distribution of methane oxidation and methanotrophic response to elevated methane concentrations in stratified waters of the Arctic fjord Storfjorden (Svalbard, Norway). *Biogeosciences* **10**(10): 6267–6268. DOI: https://doi.org/10.5194/bg-10-6267-2013

Monaghan, EJ and **Ruttenberg, KC.** 1999. Dissolved organic phosphorus in the coastal ocean: Reassessment of available methods and seasonal phosphorus profiles from the Eel River Shelf. *Limnol and Oceanogr* **44**(7): 1702–1714. DOI: https://doi.org/10.4319/lo.1999.44.7.1702

National Oceanic and Atmospheric Administration (NOAA). 2012. Multibeam Sonar Bathymetry Data collected aboard Okeanos Explorer (EX1203). National Centers for Environmental Information, NOAA. https://www.ngdc.noaa.gov/ships/okeanos_explorer/EX1203_mb.html accessed January 31, 2017.

Nauw, J, de Haas, H and **Rehder, G.** 2015. A review of oceanographic and meteorological controls on the North Sea circulation and hydrodynamics with a view to the fate of North Sea methane from well site 22/4b and other seabed sources. *Mar Petrol Geol* **68**: 861–882. DOI: https://doi.org/10.1016/j.marpetgeo.2015.08.007

NOAA Office of Ocean Exploration and Research. 2012. Water Column Sonar Data Collection (EX1203, EM302). National Geophysical Data Center, NOAA. accessed January 31, 2017. DOI: https://doi.org/10.7289/V5T43R1M

Paris, CB, Hénaff, ML, Aman, ZM, Subramaniam, A, Helgers, J, Wang, DP, Kourafalou, VH and **Srinivasan, A.** 2012. Evolution of the Macondo well blowout: Simulating the effects of the circulation and synthetic dispersants on the subsea oil transport. *Environ Sci Tech* **46**(24): 13293–13302. DOI: https://doi.org/10.1021/es303197h

Pedneault, E, Galand, PE, Potvin, M, Tremblay, JÉ and **Lovejoy, C.** 2014. Archaeal amoA and ureC genes and their transcriptional activity in the Arctic Ocean. *Sci Rep* **4**. DOI: https://doi.org/10.1038/srep04661

Rakowski, CV, Megan, C, Bosman, S, Rogers, KL, Gillies, LE, Chanton, JP and **Mason, OU.** 2015. Methane and microbial dynamics in the Gulf of Mexico water column. *Front Mar Sci* **2**: 69.

Reddy, CM, Arey, JS, Seewald, JS, Sylva, SP, Lemkau, KL, Nelson, RK, Carmichael, CA, McIntyre, CA, Fenwick, J, Ventura, GT, Van Mooy, BAS and **Camilli, R.** 2012. Composition and fate of gas and oil released to the water column during the Deepwater Horizon oil spill. *P Natl Acad Sci USA* **109**(50): 20229–20234. DOI: https://doi.org/10.1073/pnas.1101242108

Redmond, M and **Valentine, D.** 2012. Natural gas and temperature structured a microbial community response to the Deepwater Horizon oil spill. *P Natl Acad Sci USA* **109**: 20292–20297. DOI: https://doi.org/10.1073/pnas.1108756108

Reeburgh, W. 2007. Oceanic methane biogeochemistry. *Amer Chem Soc* **107**(2): 486–513. DOI: https://doi.org/10.1021/cr050362v

Rehder, G, Keir, RS, Suess, E and **Rhein, M.** 1999. Methane in the northern Atlantic controlled by

microbial oxidation and atmospheric history. *Geophys Res Lett* **26**(5): 587. DOI: https://doi.org/10.1029/1999GL900049

Rivers, AR, Sharma, S, Tringe, SG, Martin, J, Joye, SB and **Moran, MA.** 2013. Transcriptional response of bathypelagic marine bacterioplankton to the Deepwater Horizon oil spill. *ISME Journal* **7**(12): 2315–2329. DOI: https://doi.org/10.1038/ismej.2013.129

Roberts, HH and **Carney, RS.** 1997. Evidence of episodic fluid, gas, and sediment venting on the northern Gulf of Mexico continental slope. *Econ Geol* **92**(7–8): 863–879. DOI: https://doi.org/10.2113/gsecongeo.92.7-8.863

Roberts, HH, McBride, RA and **Coleman, JM.** 1999. Outer shelf and slope geology of the Gulf of Mexico: An overview. *The Gulf of Mexico Large Marine Ecosystem: Blackwell Science*.

Rolling Deck to Repository (R2R) Program. 2012. Water Column Sonar Data Collection (FK006B, EM302). National Centers for Environmental Information, NOAA, accessed February 22, 2017.

Rolling Deck to Repository (R2R) Program. 2013. Water Column Sonar Data Collection (AT26-13, EM122). National Centers for Environmental Information, NOAA, accessed February 16, 2017.

Rubin-Blum, M, Anthony, CP, Borowski, C, Sayavedra, L, Pape, T, Sahling, H, Borhmann, G, Kliener, M, Redmond, MC, Valentine, DL and **Dubilier, N.** 2017. Short-chain alkanes fuel mussel and sponge *Cycloclasticus* symbionts from deep-sea gas and oil seeps. *Nat Microbiol* **2**: 17092. DOI: https://doi.org/10.1038/nmicrobiol.2017.93

Sandbeck, KA and **Reeburgh, WS.** 1989. Microbiological preparation of ^{3}H-labelled methane. *J Labelled Compd Rad* **27**(11): 1285–1291. DOI: https://doi.org/10.1002/jlcr.2580271107

Sauter, EJ, Muyakshin, SI, Charlou, JL, Schlüter, M, Boetius, A, Jerosch, K, Damm, E, Foucher, J-P and **Klages, M.** 2006. Methane discharge from a deep-sea submarine mud volcano into the upper water column by gas hydrate-coated methane bubbles. *Earth Planet Sci Lett* **243**(3–4): 354–365. DOI: https://doi.org/10.1016/j.epsl.2006.01.041

Schmitt, M, Faber, E, Botz, R and **Stoffers, P.** 1991. Extraction of methane from seawater using ultrasonic vacuum degassing. *Anal Chem* **63**(5): 529–532. DOI: https://doi.org/10.1021/ac00005a029

Scranton, MI and **Brewer, PG.** 1978. Consumption ofdissolved methane in the deep ocean. *Limnol Oceanogr* **23**(6): 1207–1213. DOI: https://doi.org/10.4319/lo.1978.23.6.1207

Shiller, AM and **Joung, D.** 2012. Nutrient depletion as a proxy for microbial growth in Deepwater Horizon subsurface oil/gas plumes. *Environ Res Lett* **7**(4). DOI: https://doi.org/10.1088/1748-9326/7/4/045301

Sieburth, JN, Johnson, PW, Eberhardt, MA, Sieracki, ME, Lidstrom, M and **Laux, D.** 1987. The first methane-oxidizing bacterium from the upper mixing layer of the deep ocean: *Methylomonas pelagica* sp. nov. *Curr Microbiol* **14**(5): 285–293. DOI: https://doi.org/10.1007/BF01568138

Solomon, EA, Kastner, M, MacDonald, IR and **Leifer, I.** 2009. Considerable methane fluxes to the atmosphere from hydrocarbon seeps in the Gulf of Mexico. *Nat Geosci* **2**(8): 561–565. DOI: https://doi.org/10.1038/ngeo574

Solórzano, L. 1969. Determination of ammonia in natural waters by the phenolhypochlorite method. *Limnol Oceanogr* **14**(5): 799–801. DOI: https://doi.org/10.4319/lo.1969.14.5.0799

Solórzano, L and **Sharp, JH.** 1980. Determination of total dissolved phosphorus particulate phosphorus in natural water. *Limnol Oceanogr* **25**(4): 754–758. DOI: https://doi.org/10.4319/lo.1980.25.4.0754

Steinle, L, Graves, CA, Treude, T, Ferré, B, Biastoch, A, Bussmann, I, Berndt, C, Krastel, S, James, RH, Behrens, E, Böning, CW, Greinert, J, Sapart, C-J, Scheinert, M, Sommer, S, Lehmann, MF and **Niemann, H.** 2015. Water column methanotrophy controlled by a rapid oceanographic switch. *Nat Geosci* **8**: 1–6. DOI: https://doi.org/10.1038/ngeo2420

Steinle, L, Schmidt, M, Bryant, L, Haeckel, M, Linke, P, Sommer, S, Zopfi, J, Lehmann, MF, Treude, T and **Niemann, H.** 2016. Linked sediment and water-column methanotrophy at a man-made gas blowout in the North Sea: Implications for methane budgeting in seasonally stratified shallow seas. *Limnol Oceanogr* **61**: S367–S386. DOI: https://doi.org/10.1002/lno.10388

Tavormina, PL, Ussler, W, Steele, JA, Connon, SA, Klotz, MG and **Orphan, VJ.** 2013. Abundance and distribution of diverse membrane-bound monooxygenase (Cu-MMO) genes within the Costa Rica oxygen minimum zone. *Env Microbiol Rep* **5**(3): 414–423. DOI: https://doi.org/10.1111/1758-2229.12025

Torres, ME, McManus, J, Hammond, DE, De Angelis, MA, Heeschen, KU, Colbert, SL, Tryon, MD, Brown, KM and **Suess, E.** 2002. Fluid and chemical fluxes in and out of sediments hosting methane hydrate deposits on Hydrate Ridge, OR, I: Hydrological provinces. *Earth Planet Sci Lett* **201**(3–4): 525–540. DOI: https://doi.org/10.1016/S0012-821X(02)00733-1

UNOLS R2R. 2012. Multibeam Sonar Bathymetry Data collected aboard Falkor (FK006B). National Centers for Environmental Information, NOAA. https://www.ngdc.noaa.gov/ships/falkor/FK006B_mb.html accessed February 22, 2017. Bathymetry Data Identifier: gov.noaa.ngdc.mgg.multibeam:FK006B_Multibeam.

UNOLS R2R. 2014. Multibeam Sonar Bathymetry Data collected aboard Atlantis (AT26-13). National Centers for Environmental Information, NOAA. https://www.ngdc.noaa.gov/ships/atlantis/AT26-13_mb.html accessed February 16, 2017. Bathymetry Data Identifier: gov.noaa.ngdc.mgg.multibeam:AT26-13_Multibeam.

Valentine, DL, Blanton, D, Reeburgh, W and **Kastner, M.** 2001. Water Column methane oxidation adjacent to an area of active hydrate dissociation, Eel River Basin. *Geochim Cosmochim Ac* **65**(16): 63–86. DOI: https://doi.org/10.1016/j.cognition.2008.05.007

Valentine, DL, Kessler, JD, Redmond, MC, Mendes, SD, Heintz, MB, Farwell, C, Hu, L, Kinnaman, FS, Yvon-Lewis, S, Du, M, Chan, EW, Tigreros, FG and **Villanueva, CJ.** 2010. Propane respiration jump-starts microbial response to a deep oil spill. *Science*, **330**(6001): 208–211. DOI: https://doi.org/10.1126/science.1196830

Wankel, SD, Joye, SB, Samarkin, VA, Shah, SR, Friederich, G, Melas-Kyriazi, J and **Girguis, PR.** 2010. New Constraints on methane fluxes and rates of anaerobic methane oxidation in a Gulf of Mexico brine pool via *in situ* mass spectrometry. *Deep-Sea Res II: Tropical Studies in Oceanography* **57**(21–23): 2022–2029. DOI: https://doi.org/10.1016/j.dsr2.2010.05.009

Ward, BB, Kilpatrick, KA, Novelli, PC and **Scranton, MI.** 1987. Methane oxidation and methane fluxes in the ocean surface layer and deep anoxic waters. *Nature* **327**(6119): 226–229. DOI: https://doi.org/10.1038/327226a0

Wilkins, D, Van Sebille, E, Rintoul, SR, Lauro, FM and **Cavicchioli, R.** 2013. Advection shapes Southern Ocean microbial assemblages independent of distance and environment effects. *Nat Commun* **4**: 1–7. DOI: https://doi.org/10.1038/ncomms3457

Wilson, A and **Ruppel, C.** 2007. Salt tectonics and shallow subseafloor fluid convection: Models of coupled fluid-heat-salt transport. *Geofluids* **7**(4): 377–386. DOI: https://doi.org/10.1111/j.1468-8123.2007.00191.x

Wise, MG, Mcarthur, JV and **Lawrence, J.** 1999. Methanotroph diversity in landfill soil: Isolation of novel type I and type II methanotrophs whose presence was suggested by culture-independent 16S ribosomal DNA analysis. *Appl Environ Microb* **65**(11): 4887–4897.

Yang, T, Nigro, LM, Gutierrez, T, D'Ambrosio, L, Joye, SB, Highsmith, R and **Teske, A.** 2016. Pulsed blooms and persistent oil-degrading bacterial populations in the water column during and after the Deepwater Horizon blowout. *Deep-Sea Res Part II: Topical Studies in Oceanography* **129**: 282–291. DOI: https://doi.org/10.1016/j.dsr2.2014.01.014

How to cite this article: Rogener, MK, Bracco, A, Hunter, KS, Saxton, MA and Joye, SB. 2018. Long-term impact of the Deepwater Horizon oil well blowout on methane oxidation dynamics in the northern Gulf of Mexico. *Elem Sci Anth,* 6: 73. DOI: https://doi.org/10.1525/elementa.332

Domain Editor-in-Chief: Jody W. Deming, Ph.D., Department of Biological Oceanography, University of Washington, US

Associate Editor: Jeff Bowman, University of California San Diego Scripps Institution of Oceanography, US

Knowledge Domain: Ocean Science

Part of an *Elementa* Special Feature: Impacts of Natural Versus Anthropogenic Oil Inputs on the Gulf of Mexico Ecosystem

Submitted: 09 June 2018 **Accepted:** 12 October 2018 **Published:** 07 December 2018

ELEMENTA Science of the Anthropocene

Elem Sci Anth is a peer-reviewed open access journal published by University of California Press.

OPEN ACCESS